**Template-assisted $SnO_2$: synthesis, composition and photoelectrocatalytical properties**

Evgenii Gribov[1,2*], Evgeny Koshevoy[1], Iulia Chikunova[1] and Valentin Parmon[1]

[1]Boreskov Institute of Catalysis SB RAS, Pr. Ak. Lavrentieva, 5, Novosibirsk, 630090, Russia

[2]Novosibirsk State University, Pirogova, 1, Novosibirsk, 630090, Russia

*Correspondence: gribov@catalysis.ru

# Supporting information

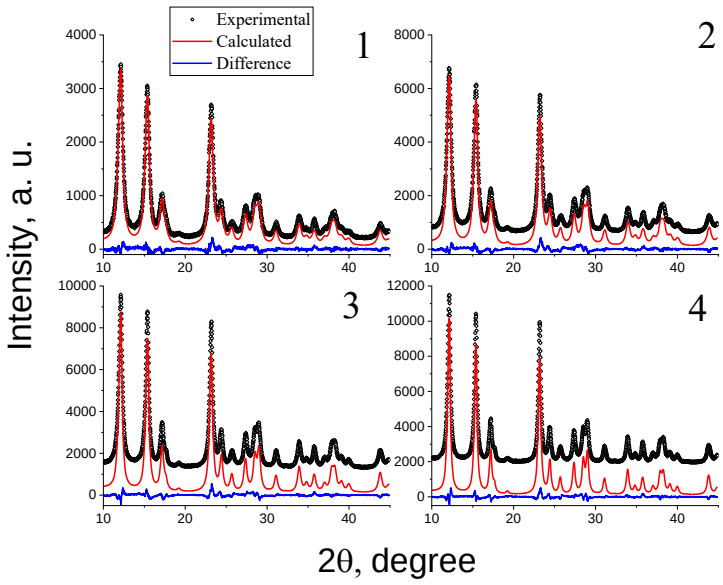


**Figure S1**. XRD data for samples TO1 (1), TO2 (2), TO3 (3) and TO4 (4). Diamond – Experimental curves, Red lines – Calculated curves, Blue lines – Difference.

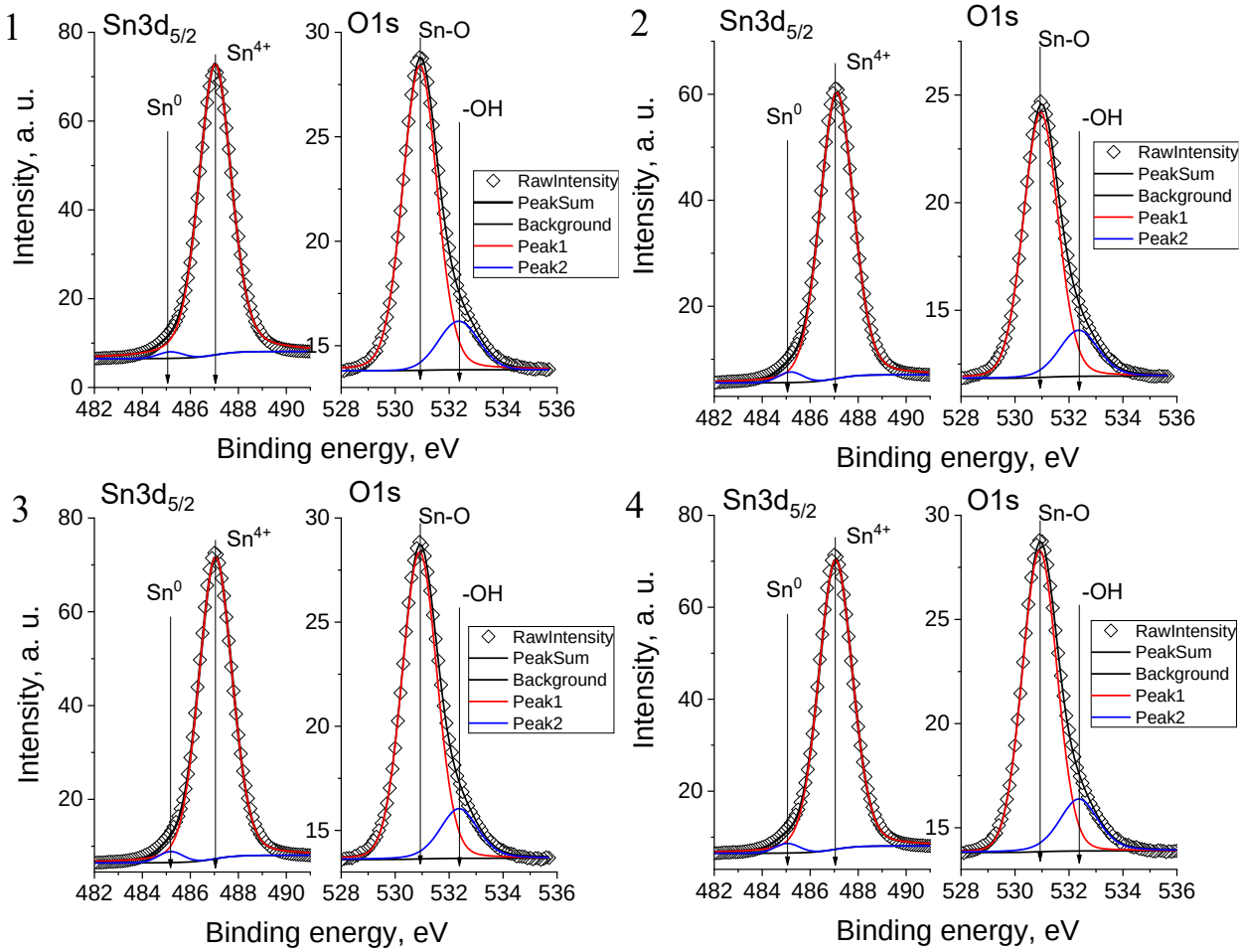


**Figure S2**. XPS data of samples TO1 (1), TO2 (2), TO3 (3) and TO4 (4) with peak decompositions for $Sn3d_{5/2}$ and O1s.

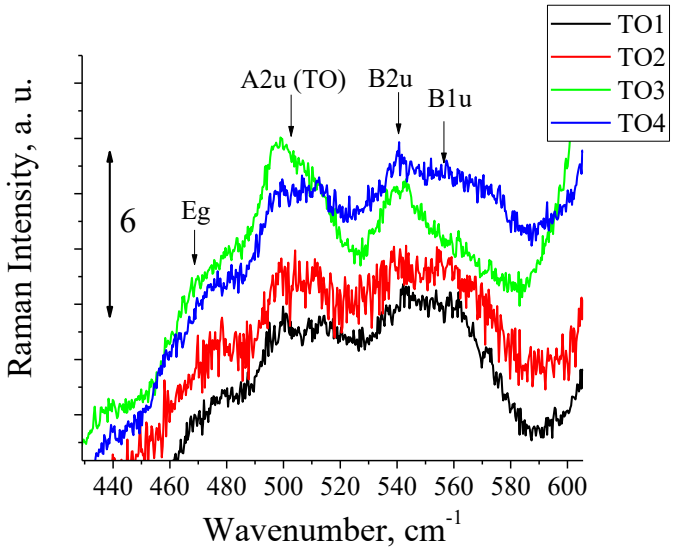


**Figure S3**. Raman spectra of samples in the region 440-600 $cm^{-1}$.

**Table S1**. Comparison of bands in Raman spectra with literature data.

| Phase | Vibrations | TO1 | TO2 | TO3 | TO4 | References |
|---|---|---|---|---|---|---|
| SnO | B1g | 107 | 107 | 107 | 107 | 107-109[1], 111[5], 113[6] |
| SnO | A1g | - | - | 218 | 220 | 211[6] |
| $SnO_2$ | Eu(1)-TO | 249 | 249 | 249 | 249 | 244[2], 248[4] |
| $SnO_2$ | Eu(2)-TO | 300 | 300 | 300 | 300 | 293[2] |
| $SnO_2$ | Eu(2)-LO | 312 | 312 | 312 | 312 | 306[2] |
| $SnO_2$ | A2g | 347 | 347 | 347 | 347 | 360[2] |
| $SnO_2$ | Eg | 472 | 472 | 472 | 472 | 477[1,2,4] |
| $SnO_2$ | 499 | 496 | 496 | 496 | 496 | 504[1], 510[4] |
| $SnO_2$ | B2u | 543 | 543 | 543 | 543 | 542[1] |
| $SnO_2$ | B1u | 562 | 562 | 562 | 562 | 564[2] |
| $SnO_2$ | A1g | 625 | 625 | 623 | 625 | 636[1-3], 630[4] |
| $SnO_2$ | A2u-LO | 691 | 691 | 684 | 691 | 697[1], 681[4] |
| $SnO_2$ | B2g | 762 | 762 | 762 | 762 | 778[1], 762[4] |

[1] Gaur, L.K., Chandra Mathpal, M., Kumar, P., Gairola, S.P., Agrahari, V., Martinez, M.A.R., Aragon, F.F.H., Soler, M.A.G., Swart, H.C., Agarwal, A. Observations of phonon anharmonicity and microstructure changes by the laser power dependent Raman spectra in Co doped $SnO_2$ nanoparticles // J Alloys Compd. - 2020. - V. 831. – P. 154836.

[2] Lan, T., Li, C.W., Fultz, B. Phonon anharmonicity of rutile $SnO_2$ studied by Raman spectrometry and first principles calculations of the kinematics of phonon-phonon interactions // Physical Review B - Condensed Matter and Materials Physics. - 2012. - V. 86. - P. 134302.

[3] Xiong, C., Xiong, Y., Zhu, H., Zhang, Y., Liu, Y. Investigation of Raman spectrum for nano-$SnO_2$ // Science in China, Series A: Mathematics, Physics, Astronomy. - 1997. - V. 40. - P. 1222-1227.

[4] Babu, B., Talluri, B., Gurugubelli, T.R., Kim, J., Yoo, K. Effect of annealing environment on the photoelectrochemical water oxidation and electrochemical supercapacitor performance of $SnO_2$ quantum dots // Chemosphere. - 2022. - V. 286. - P. 131577.

[5] Zaraska, L., Gawlak, K., Wiercigroch, E., Malek, K., Kozieł, M., Andrzejczuk, M., Marzec, M.M., Jarosz, M., Brzózka, A., Sulka, G.D. The effect of anodizing potential and annealing conditions on the morphology, composition and photoelectrochemical activity of porous anodic tin oxide films // Electrochim Acta. - 2019. - V. 319. - P. 18-30.

[6] Batzill, M., Diebold, U. The surface and materials science of tin oxide // Progress in Surface Science. - 2005. - V. 79. - P. 47-154.

Flat-band determination of samples obtained from photocurrent beginning by comparing of cyclic voltammograms (CV) curves measured in light (370 nm) and dark for cathodic and anodic scans.

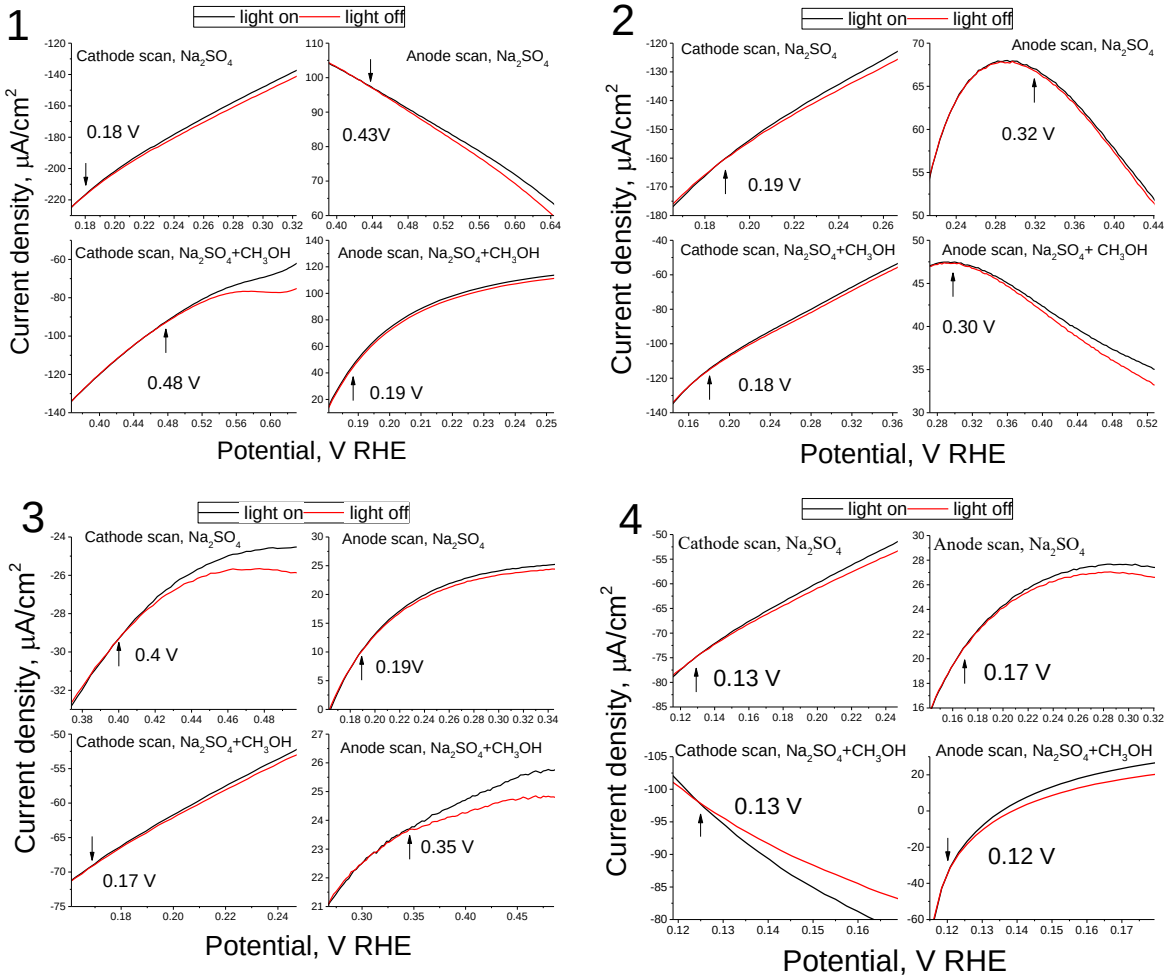


**Figure S4**. Current curves of CV (scan rate – 10 mV/s) in dark (black) and under irradiation (red) for the samples TO1 (1), TO2 (2), TO3 (3) и TO4 (4) in electrolyte (upper plots) and with methanol addition (lower plots). Arrows show photocurrent onset potential (pointed by numbers).

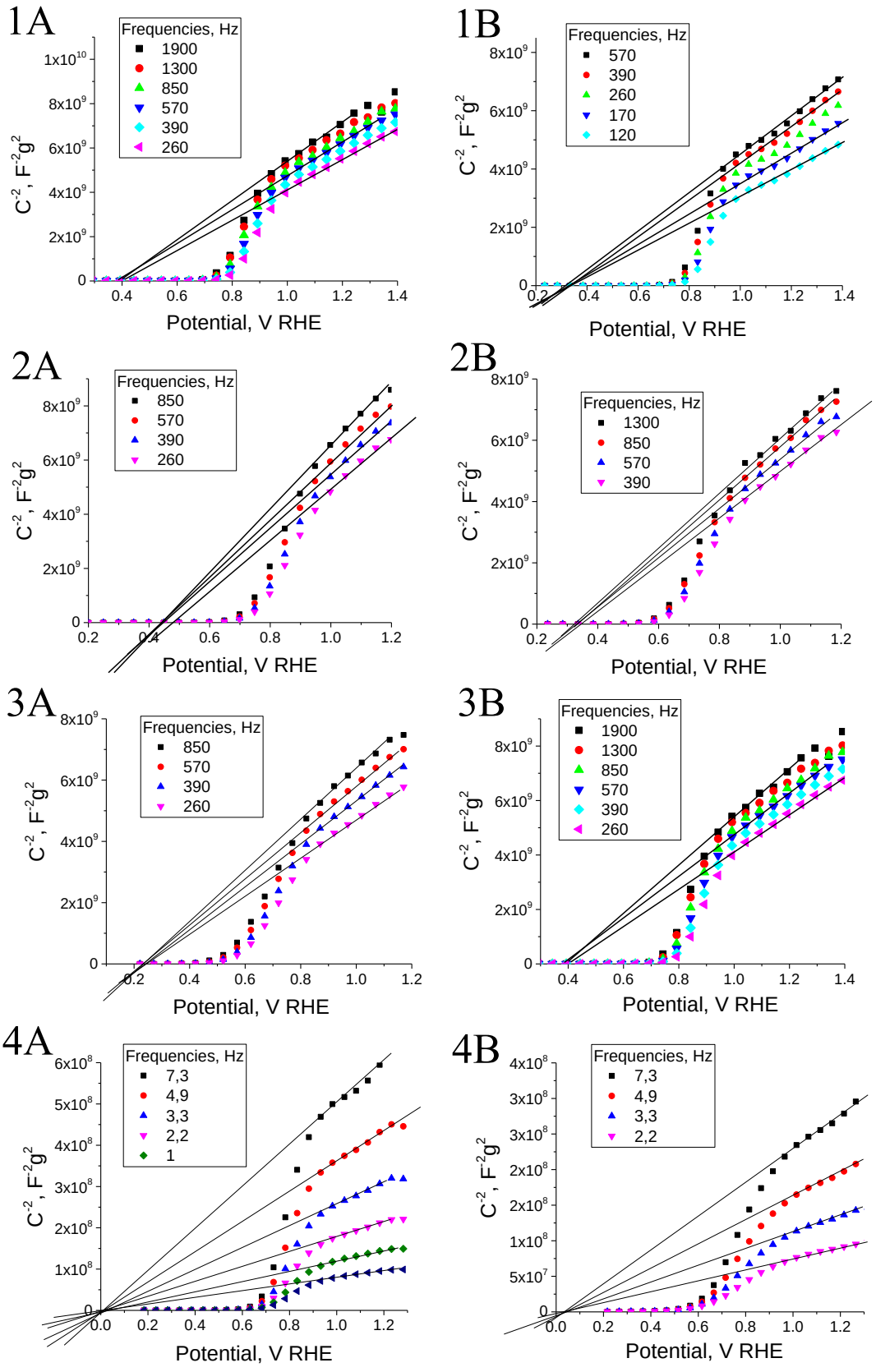


**Figure S5**. Mott-Schottky plots for dark capacity measurements of samples: TO1 (1), TO2 (2), TO3 (3) и TO4 (4) in electrolyte (A) and with methanol addition (B). The frequencies were chosen, which data linear approximations make one-point intercept.

Flat-band determination of samples obtained from open circuit potential dependence on irradiation intensity (370 nm). Flat-band potentials were determined from extrapolation of OCP dependence to infinite intensity and introducing of methanol as sacrificial agent give more reliable results.

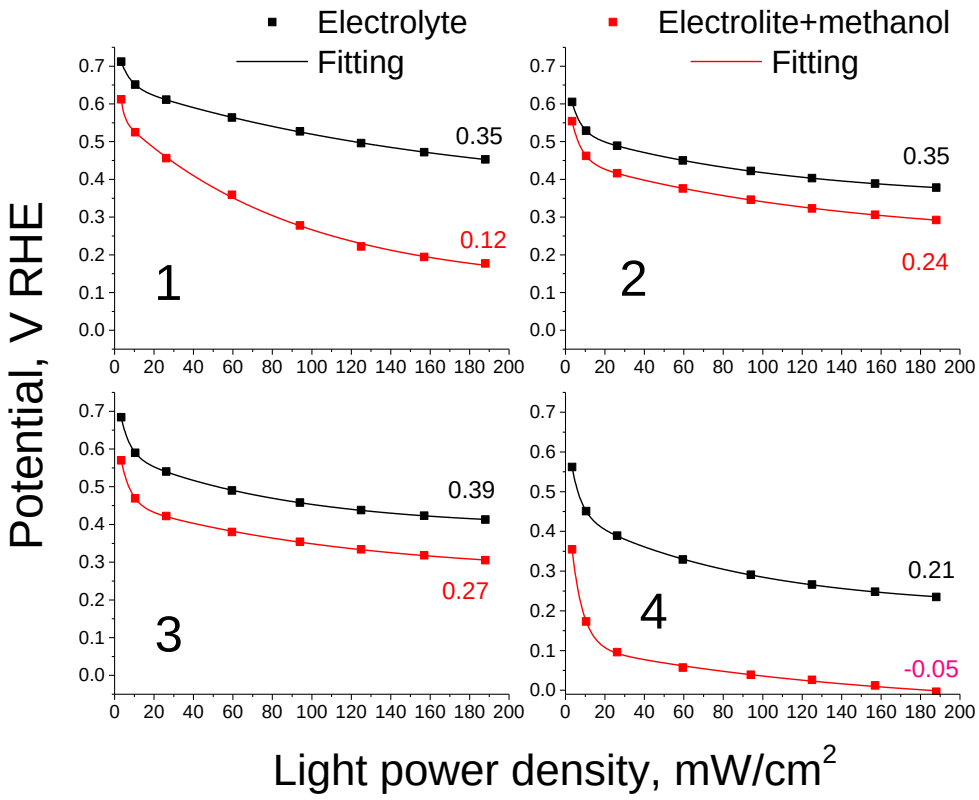


**Figure S6**. Open circuit potential dependence from light irradiation intensity for samples TO1 (1), TO2 (2), TO3 (3) и TO4 (4) in electrolyte (black points) and with methanol addition (red points). For estimation of the potentials at infinite intensity (pointed by numbers) the dependencies were approximated by biexponential curves.

Flat-band determination of samples obtained from photocurrent onset at chopped illumination. Flat-band potential was fixed when photocurrents fade. Hovewer, photoreduction of samples especially in presence of methanol may hamper analysis, makes it unsuitable in case of TO4 (fig. S7(4b)).

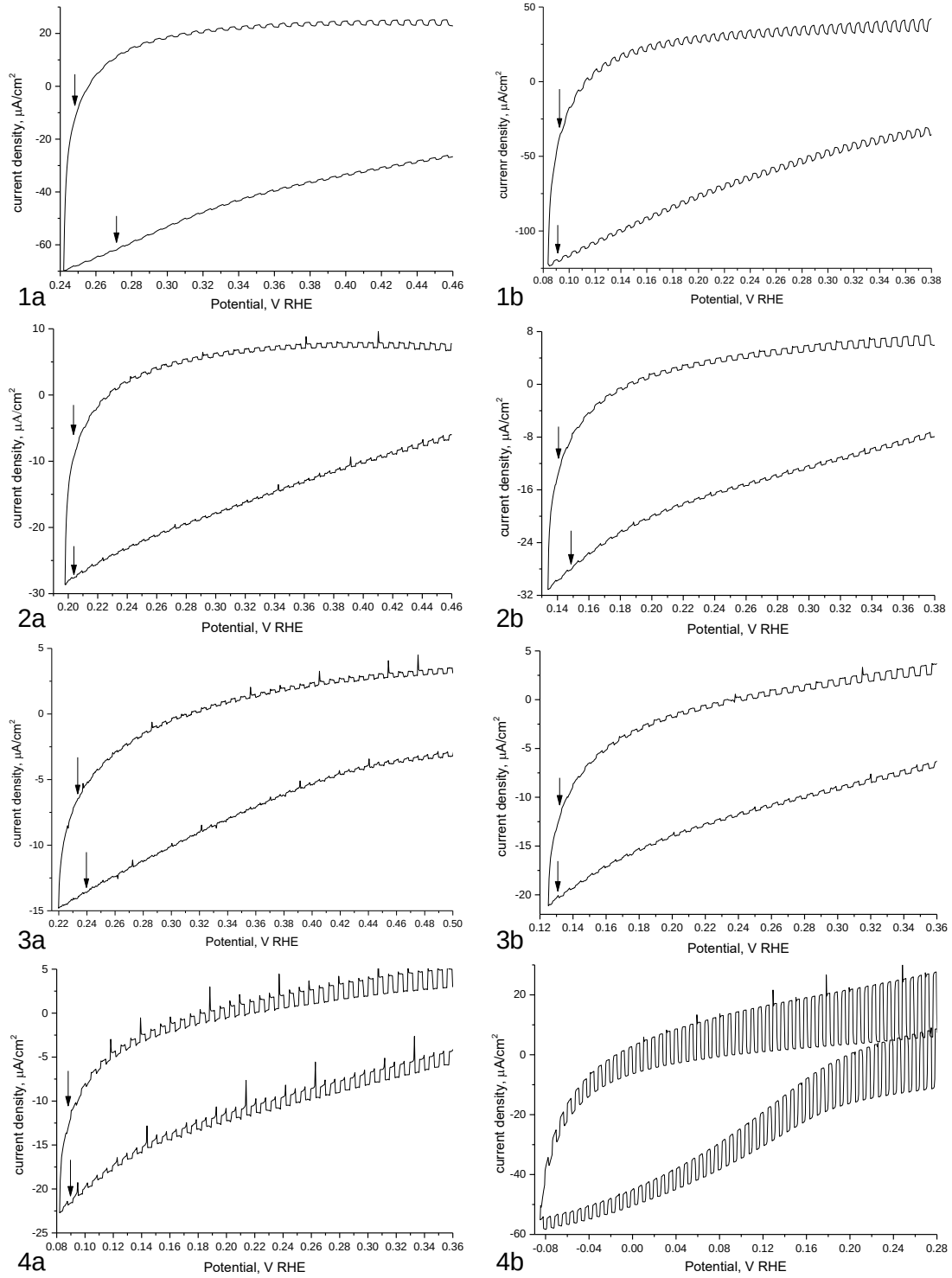


**Figure S7**. Current curves of CV (scan rate – 1 mV/s) at chopped illumination (3 s) for the samples TO1 (1), TO2 (2), TO3 (3) и TO4 (4) in electrolyte (a) and with methanol addition (b). Arrows show photocurrent onset potential.

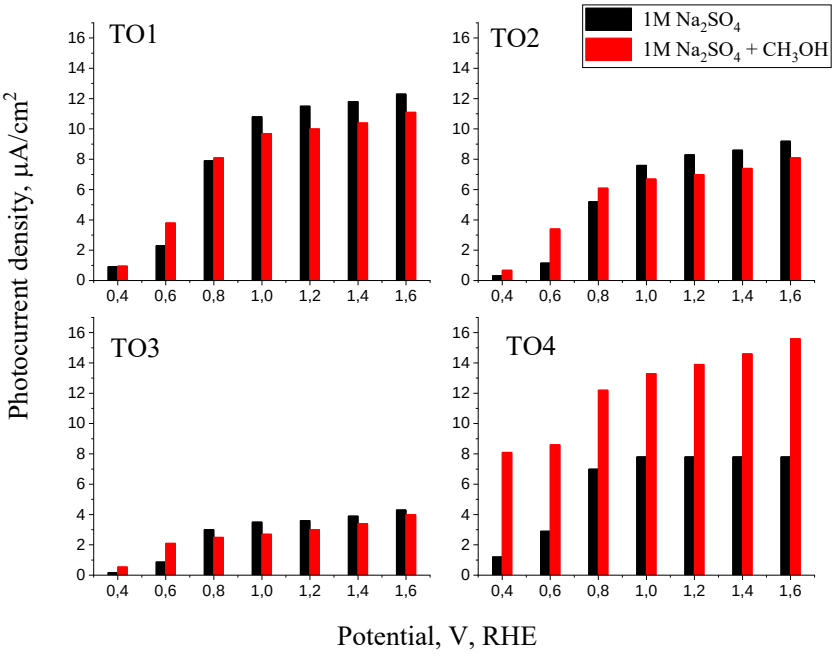


**Figure S8**. Dependence of photocurrent density from potential in electrolyte (black) and with methanol addition (red) for the samples TO1–TO4.

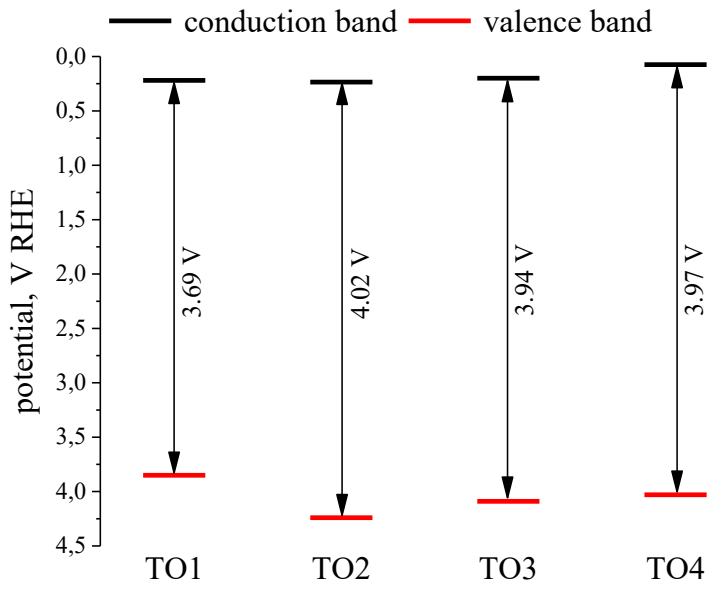


**Figure S9**. Energy band diagram of samples based on average flat-band potentials and band gaps for direct transitions.